

Broadening not strengthening of the Agulhas Current since the early 1990s

Lisa M. Beal¹ & Shane Elipot¹

Western boundary currents—such as the Agulhas Current in the Indian Ocean—carry heat poleward, moderating Earth's climate and fuelling the mid-latitude storm tracks^{1,2}. They could exacerbate or mitigate warming and extreme weather events in the future, depending on their response to anthropogenic climate change. Climate models show an ongoing poleward expansion and intensification of the global wind systems, most robustly in the Southern Hemisphere^{3–5}, and linear dynamical theory^{6,7} suggests that western boundary currents will intensify and shift poleward as a result^{3,8}. Observational evidence of such changes comes from accelerated warming and air–sea heat flux rates within all western boundary currents, which are two or three times faster than global mean rates^{5,9,10}. Here we show that, despite these expectations, the Agulhas Current has not intensified since the early 1990s. Instead, we find that it has broadened as a result of more eddy activity. Recent analyses of other western boundary currents—the Kuroshio and East Australia currents—hint at similar trends^{11–15}. These results indicate that intensifying winds may be increasing the eddy kinetic energy of boundary currents, rather than their mean flow. This could act to decrease poleward heat transport and increase cross-frontal exchange of nutrients and pollutants between the coastal ocean and the deep ocean. Sustained *in situ* measurements are needed to properly understand the role of these current systems in a changing climate.

To estimate the trend in Agulhas Current transport we build a 22-year proxy using three years of *in situ* measurements from the Agulhas Current Time-series (ACT) array¹⁶ combined with coincident along-track satellite altimeter data spanning the years 1993–2015 (Fig. 1).

We define two measures of transport for the Agulhas Current: a streamwise, southwestward jet transport T_{jet} , and a geographically fixed, net boundary-layer transport T_{box} . Over the three years of *in situ* data the mean and standard deviation of T_{jet} are -84 Sv ($1 \text{ Sv} = 10^6 \text{ m}^3 \text{ s}^{-1}$) and 24 Sv, respectively, and of T_{box} are -77 Sv and 32 Sv, respectively¹⁶. In past studies T_{box} has been more often applied to quantify boundary current flow, yet this measure suffers spurious effects from meander events¹⁶, which are largely removed in the streamwise case.

Before building a proxy we first test for the necessary condition of a linear and fixed relationship between our *in situ* transports and sea surface slope from satellite altimeter. Sea surface slope is equivalent to surface geostrophic velocity, and on the basis of previous analyses we expect the relationship between surface geostrophic velocity and full-depth transport to be strong in the Agulhas Current, despite the presence of an undercurrent^{17,18}. Using empirical orthogonal function (EOF) analysis, we find that transport and sea surface height and slope along the ACT array do exhibit similar and significantly correlated modes of variance (correlations >0.7 , P values $<10^{-3}$). In each case, these modes express weakening or strengthening, broadening or narrowing, and meandering of the Agulhas Current jet (Extended Data Fig. 1 and Methods). Hence, variance of the sea surface is strongly tied to oceanic transport along the ACT array at 34° S and

using altimetry to build a proxy for Agulhas Current transport seems physically justifiable.

For our Agulhas Current transport proxy we build nine linear regression models between sea surface slope and transport per unit distance T_x , one at each of the ACT mooring locations (Fig. 1). We then fit a smoothed function at 1-km intervals and integrate horizontally to obtain T_{jet} and T_{box} for each altimeter pass. In this way, we can account for a current that meanders and changes in width by allowing the core and flanks of the flow to vary at different rates, although the vertical structure necessarily remains fixed. A proxy based on regression between array-wide sea level variance and total transport is more statistically successful for T_{box} ; however, we find that this proxy's trend is spurious because of the observed broadening of the current (Extended Data Fig. 2 and Methods).

Our 22-year proxy time series are shown in Fig. 2, together with their frequency spectra and seasonal cycles. For T_{box} our proxy explains 61% of the variance during the ACT period, while for T_{jet} it explains 55% of the variance. The jet and boundary layer transports have spectral peaks that are significant (see Methods subsection 'Spectral Estimates') at the annual period (Fig. 2c) and their seasonal cycles match those of the *in situ* data¹⁶, with weakest transports occurring during austral winter, in August, and strongest transports occurring throughout austral summer (Fig. 2d). At most timescales, the variance of T_{jet} is less than that of T_{box} (Fig. 2c and d).

The long-term trends are $+1.0 \pm 2.4$ Sv per decade for T_{box} and $+2.1 \pm 2.1$ Sv per decade for T_{jet} (where tolerances are the 95% confidence interval). These trends would correspond to a slight decrease in Agulhas Current transport, although neither trend is significant. In the Indian Ocean, a spin-up of the ocean circulation over the northern reaches of the subtropical gyre has been implied by a small intensification of the trade winds⁴ and an increase in the Indonesian through-flow¹⁹ since the early 1990s. Farther south at the ACT array the trend in wind stress curl is less certain, since changes in the strength and latitudinal position of the Westerlies differ between wind products²⁰. Nevertheless, the derived winds from the 20CRv2 reanalysis show an upward trend in wind curl over all the southern subtropical oceans²¹, and rapidly increasing sea surface temperatures and air–sea fluxes have been attributed to a strengthening and poleward shift of the Agulhas Current^{5,9,10}.

Given that our results appear to contrast with these indicators, we examine our proxy trends more closely. We look at the structure of sea level and slope trends along the ACT array (Fig. 3a and b) and compare them to our transport trend. We find a non-uniform pattern of sea level rise across the Agulhas Current, with a minimum at 130 km from the coast (Fig. 1). This pattern gives rise to a negative trend in sea surface slope across the inshore half of the boundary layer and a positive trend offshore (Fig. 3b). Since the mean sea surface slope is positive across the Agulhas Current (Extended Data Fig. 1), these trends result in weaker velocities within the core of the current and stronger velocities over its flank. The effect on the Agulhas Current is a weakening and broadening of the jet, as illustrated by the change in T_x across the array

¹Rosenstiel School of Marine and Atmospheric Science, University of Miami, 4600 Rickenbacker Causeway, Miami, Florida, USA.

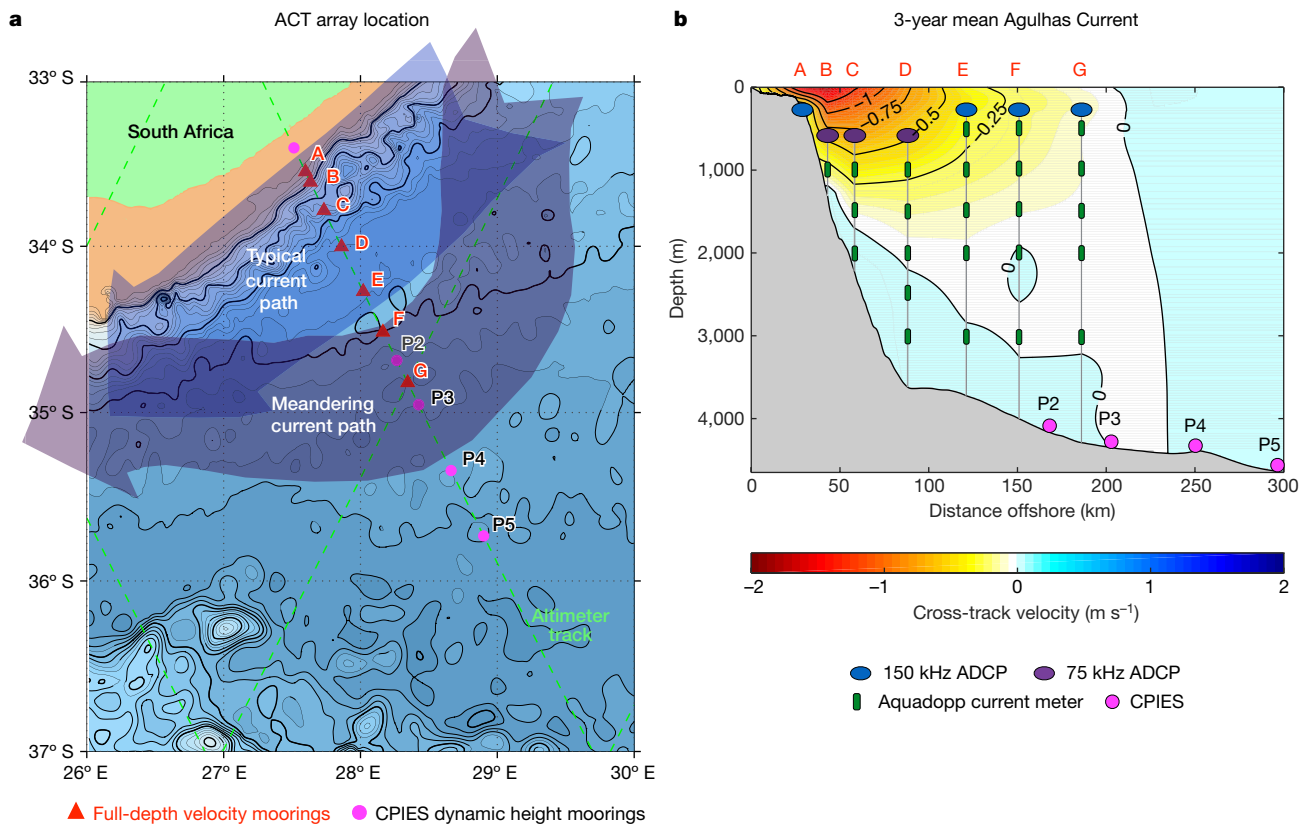


Figure 1 | Agulhas Current Time-series (ACT) instrumental array and mean Agulhas Current from April 2010 to February 2013. **a**, Geographical location of ACT mooring array, consisting of current meter moorings A–G and CPIES (Current Pressure Inverted Echo Sounders) sites P2–P5. Bathymetry down to 1,000 m is shown in tan and in deepening shades of blue thereafter, with contours every 200 m and thick contours every 1,000 m, from 200 m to 5,000 m. **b**, Vertical section

of the mooring array superposed on the 3-year mean cross-track velocity. Bathymetry is shaded grey. Southwestward velocities (Agulhas Current) are shaded yellow through to red and northeastward velocities are shaded blue (see colour scale). Acoustic Doppler Current Profilers (ADCPs) measure velocity throughout the upper water column. Aquadopp current meters measure velocity at a single point. Pairs of CPIES estimate profiles of geostrophic velocity.

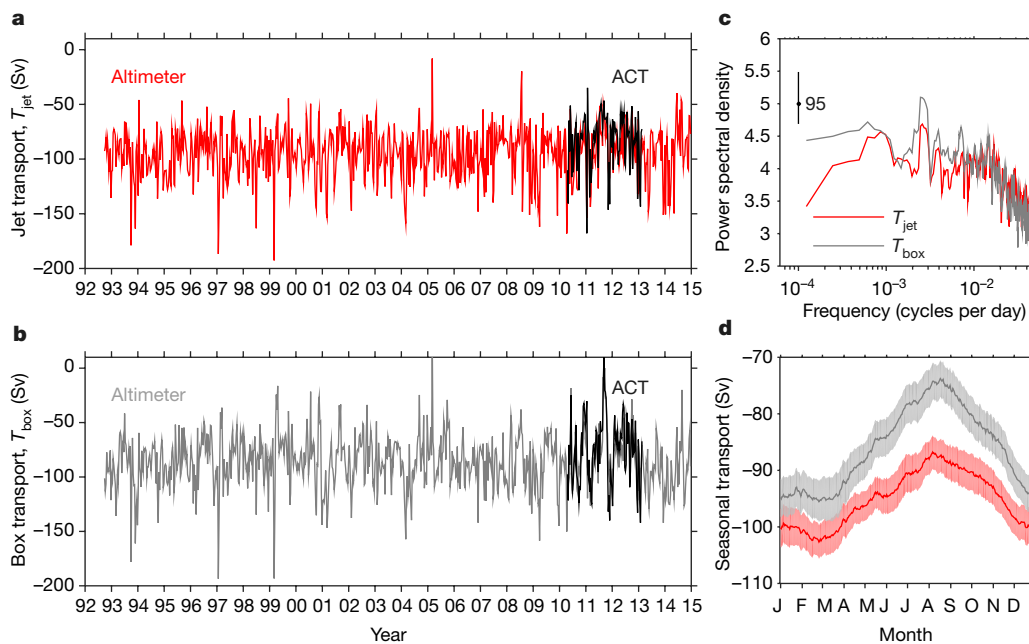


Figure 2 | Agulhas Current transport proxies based on regressions between transport and sea surface slope at each ACT mooring location. **a**, Proxy time series for jet or stream-wise transport T_{jet} . **b**, Proxy time series for boundary layer transport T_{box} . The three years of *in situ* transports from the ACT array are shown as black lines. **c**, Frequency

spectra of the jet (red) and boundary layer (grey) proxies. The 95% confidence interval is shown. **d**, Seasonal transport (daily average values) of the jet (red) and boundary layer (grey) proxies. Shading shows 95% confidence intervals.

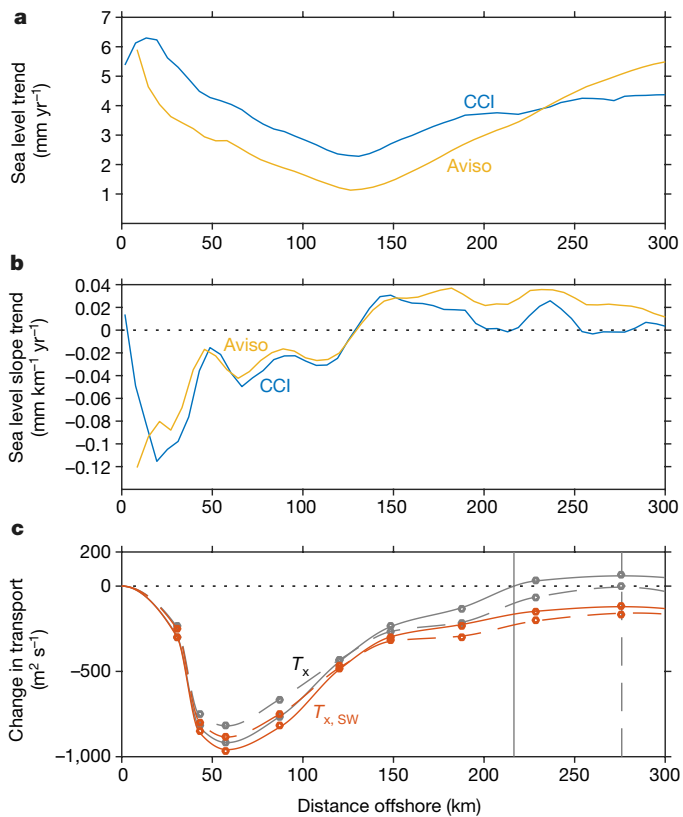


Figure 3 | Trends of sea level and oceanic transport across the Agulhas Current, showing broadening. **a**, **b**, Sea level (a) and sea surface slope (b) linear trends estimated using along-track satellite altimeter from Aviso (blue) and CCI (orange) products (1993–2015). **c**, Transport per unit distance based on regressions between sea surface slope and oceanic transport at each ACT mooring site (circles). Transport changes between the beginning (solid lines) and end (dashed lines) of the altimeter record are implied by the linear trends. T_x is net transport per unit distance and $T_{x,sw}$ is its southwestward component (as used to calculate T_{jet}). Vertical lines indicate the width of the boundary layer at the beginning (solid) and end (dashed) of the altimeter record.

from the regression models at each mooring (Fig. 3c). The core of the current is in the same position, but weaker, while flow throughout the offshore flank of the current is stronger. The resultant broadening of the boundary layer, defined by the zero crossing of T_x , is about 50 km (Fig. 3c). Hence, we conclude that the Agulhas Current is weakening and broadening over time, while its total transport remains stable.

Broadening of the Agulhas Current can be understood in the context of a simple Munk model²², whereby the width of the western boundary layer will increase if the lateral viscosity increases. This could occur as a result of an increase in eddy activity in the current over time (Fig. 4). We derive the trend in eddy kinetic energy (EKE) of the Agulhas Current at this latitude from a mapped altimeter product using a fixed number of satellites over time, as has been done previously²⁰. Consistent with this model, the trend in EKE is everywhere positive across the current, while the peak in mean kinetic energy (MKE) within the core of the jet is decreasing (Fig. 4).

Broadening can also be understood in terms of meandering. Mesoscale meanders dominate the variance—and therefore the EKE—of the Agulhas Current²³, growing largely through a barotropic conversion of energy from the mean horizontal flow^{17,18}. Such instabilities act to transfer energy offshore and decelerate the core of the jet²⁴. Hence, a reported increase in the number of meander events over time¹⁷ will lead to a weakening and broadening of the flow.

Measurements in other western boundary currents also point to trends of increasing EKE, rather than increasing transports, as we observe in the Agulhas Current. In the Pacific Ocean, there is an

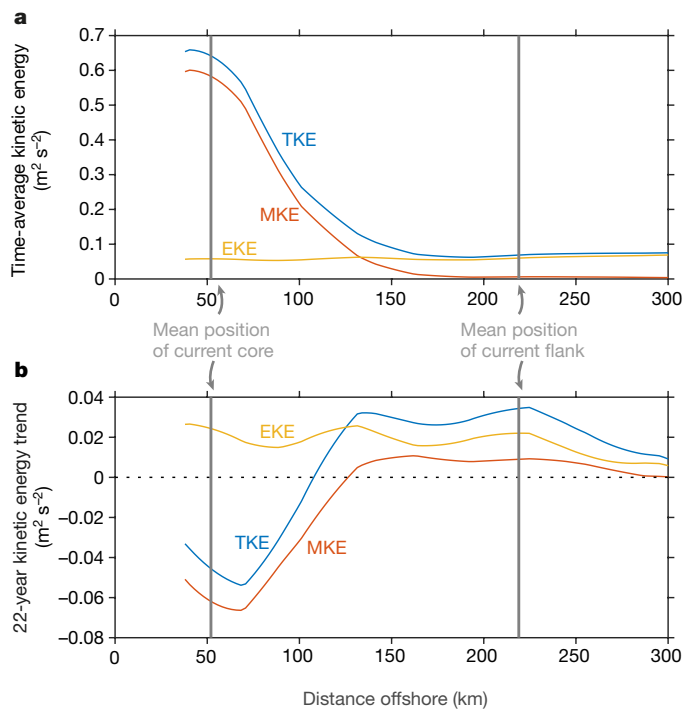


Figure 4 | Kinetic energy analyses across the Agulhas Current, showing increased eddying. **a**, Total kinetic energy (TKE), mean kinetic energy (MKE) and eddy kinetic energy (EKE) from the mapped Aviso altimeter product. Mean and eddy kinetic energies are defined as variability at timescales of less and more than eighteen months, respectively. **b**, TKE, MKE and EKE linear changes over 22 years. In **a** and **b** the mean position of the current core and its offshore flank during the three years of ACT are shown as vertical grey lines. Data within 40 km of the coast are not available in the mapped altimeter product.

increase in observed trade winds over the last twenty years, some of which is attributed to climate change²⁵. Increases in sea surface height over the north and south subtropical Pacific point to a concomitant intensification of the ocean gyres⁴. However, no compensating trends have been found in the transports of the Kuroshio or East Australia currents^{13,14}, even while they have been warming¹⁰. Instead, there is evidence that the Kuroshio Current is broadening, with the same pattern of sea level rise as seen across the Agulhas Current¹¹, and that eddy activity in both the Kuroshio and East Australia currents is increasing^{12–14}. Furthermore, eddy variability of the East Australia Current has recently been linked to regional wind stress curl¹⁵. In the Atlantic, prediction of trends in Gulf Stream intensity is complicated by a potential weakening of the overturning circulation²⁶ and by uncertain trends in wind curl¹⁰. Sea level changes along the east coast of the USA have been used to suggest a weakening of the Gulf Stream²⁷, but this is not corroborated by *in situ* measurements, which show no trend²⁸.

Extending (that is, using data to extend *in situ* observations back in time) and inferring ocean circulation changes using satellite altimeter data is becoming commonplace^{14,19,27}, in an attempt to understand oceanic change better despite a paucity of measurements. Our results call for caution when inferring trends in currents using sea surface height difference alone, since sea level changes may be inhomogeneous across the current (Fig. 3). The exact position of the current, and any broadening or narrowing over time, must be taken into account (see Methods). On multidecadal timescales, the implicit assumption of a fixed vertical stratification may also become problematic, as thermohaline changes become important. More hydrographic data are necessary, particularly within western boundary currents, to be able to estimate trends in stratification.

A particular weakness of our analysis is that it captures only changes in the Agulhas Current at 34° S, the location of the ACT array. Farther north, opposing trends in MKE and EKE are such that the mean flow

appears to be strengthening over time and there are fewer eddies²⁰. However, these inferences are made where the current core is within 40 km of the coast, a region of poor altimeter coverage, and are uncorroborated by *in situ* measurements. Another weakness is that wind products exhibit large discrepancies in the mean²⁹, such that temporal changes are even less reliable²⁰, and a poleward shift adds further uncertainty to any observed trend in wind stress curl⁵. Finally, a linear trend model accounts for only a small fraction of the variance in kinetic energy and transport of the Agulhas Current. 22 years of satellite observations are barely sufficient to discern anthropogenic trends, although decadal climate variability in the Indian Ocean is smaller than in the Pacific and Atlantic oceans. 50-year trends in sea surface temperature in the Indian Ocean sector are consistent with trends over the last two decades⁵.

Our results, together with recent analyses in other western boundary currents, suggest that intensifying winds may act to increase the EKE of boundary currents, rather than their mean flow. This hypothesis draws parallels with the eddy compensation hypothesis for the Antarctic Circumpolar Current in the Southern Ocean, where eddies appear to dampen the effect of increased wind energy input on the mean flow³⁰. In essence, while winds tend to accelerate the flow and steepen isopycnals, eddies mix laterally across the current to slump the isopycnals. Coupling between eddies and the atmosphere has also been shown to influence this frontal balance³¹. The implication of broadening boundary currents is a more porous divide between the continental shelves and the open ocean, leading to greater mixing and cross-frontal exchange. In the Agulhas Current, these changes could also enhance upwelling over the shelf, since the strongest upwelling events are driven by meanders. These implications are in contrast to those of an intensifying flow, which would tend to dampen cross-frontal mixing and increase meridional heat transport.

If western boundary currents are not strengthening, observed patterns of surface warming^{5,9,10} must be explained by a poleward shift of the ocean gyres. Broadening of western boundary currents and their extensions will also imprint on warming patterns and this should be considered in future analyses. Ocean reanalysis products and climate models fail to resolve western boundary currents and this could explain discrepancies among them and with our results^{5,10}.

Online Content Methods, along with any additional Extended Data display items and Source Data, are available in the online version of the paper; references unique to these sections appear only in the online paper.

Received 25 May; accepted 9 September 2016.

Published online 9 November; corrected online 21 December 2016

(see full-text HTML version for details).

- Hu, D. *et al.* Pacific western boundary currents and their roles in climate. *Nature* **522**, 299–308 (2015).
- Palter, J. B. The role of the Gulf Stream in European climate. *Annu. Rev. Mar. Sci.* **7**, 113–137 (2015).
- Cai, W. Antarctic ozone depletion causes an intensification of the Southern Ocean super-gyre circulation. *Geophys. Res. Lett.* **33**, L03712 (2006).
- McGregor, S., Gupta, A. S. & England, M. H. Constraining wind stress products with sea surface height observations and implications for Pacific Ocean sea level trend attribution. *J. Clim.* **25**, 8164–8176 (2012).
- Yang, H. *et al.* Intensification and poleward shift of subtropical western boundary currents in a warming climate. *J. Geophys. Res. Oceans* **121**, 4928–4945 (2016).
- Sverdrup, H. U. Wind-driven currents in a baroclinic ocean; with application to the equatorial currents of the eastern Pacific. *Proc. Natl Acad. Sci. USA* **33**, 318–326 (1947).
- Stommel, H. The westward intensification of wind-driven ocean currents. *Eos* **29**, 202–206 (1948).

- Saenko, O. A., Fyfe, J. C. & England, M. H. On the response of the oceanic wind-driven circulation to atmospheric CO₂ increase. *Clim. Dyn.* **25**, 415–426 (2005).
- Rouault, M., Penven, P. & Pohl, B. Warming in the Agulhas Current system since the 1980's. *Geophys. Res. Lett.* **36**, L12602 (2009).
- Wu, L. *et al.* Enhanced warming over the global subtropical western boundary currents. *Nat. Clim. Chang.* **2**, 161–166 (2012).
- Uchida, H. & Imawaki, S. Estimation of the sea level trend south of Japan by combining satellite altimeter data with *in situ* hydrographic data. *J. Geophys. Res. Oceans* **113**, C09035 (2008).
- Oliver, E. & Holbrook, N. Extending our understanding of South Pacific gyre spin-up: modeling the East Australian Current in a future climate. *J. Geophys. Res. Oceans* **119**, 2788–2805 (2014).
- Cetina-Heredia, P., Roughan, M., Van Sebille, E. & Coleman, M. Long-term trends in the East Australian Current separation latitude and eddy driven transport. *J. Geophys. Res. Oceans* **119**, 4351–4366 (2014).
- Yan, X. & Sun, C. An altimetric transport index for Kuroshio inflow northeast of Taiwan Island. *Sci. China Earth Sci.* **58**, 697–706 (2015).
- Sloyan, B. M. & O'Kane, T. J. Drivers of decadal variability in the Tasman Sea. *J. Geophys. Res. Oceans* **120**, 3193–3210 (2015).
- Beal, L. M., Elipot, S., Houk, A. & Leber, G. M. Capturing the transport variability of a western boundary jet: results from the Agulhas Current Time-Series experiment (ACT)*. *J. Phys. Oceanogr.* **45**, 1302–1324 (2015).
- Elipot, S. & Beal, L. M. Characteristics, energetics, and origins of Agulhas Current meanders and their limited influence on ring shedding. *J. Phys. Oceanogr.* **45**, 2294–2314 (2015).
- Tsugawa, M. & Hasumi, H. Generation and growth mechanism of the Natal Pulse. *J. Phys. Oceanogr.* **40**, 1597–1612 (2010).
- Sprintall, J. & Révelard, A. The Indonesian throughflow response to Indo-Pacific climate variability. *J. Geophys. Res. Oceans* **119**, 1161–1175 (2014).
- Backeberg, B. C., Penven, P. & Rouault, M. Impact of intensified Indian Ocean winds on mesoscale variability in the Agulhas system. *Nat. Clim. Chang.* **2**, 608–612 (2012).
- Compo, G. P. *et al.* The twentieth century reanalysis project. *Q. J. R. Meteorol. Soc.* **137**, 1–28 (2011).
- Munk, W. H. On the wind driven ocean circulation. *J. Meteorol.* **7**, 80–93 (1950).
- Bryden, H. L., Beal, L. M. & Duncan, L. M. Structure and transport of the Agulhas Current and its temporal variability. *J. Oceanogr.* **61**, 479–492 (2005).
- Pedlosky, J. *Geophysical Fluid Dynamics* 2nd edn (Springer, 1987).
- England, M. H. *et al.* Recent intensification of wind-driven circulation in the Pacific and the ongoing warming hiatus. *Nat. Clim. Chang.* **4**, 222–227 (2014).
- Cheng, W., Chiang, J. C. & Zhang, D. Atlantic meridional overturning circulation (AMOC) in CMIP5 models: RCP and historical simulations. *J. Clim.* **26**, 7187–7197 (2013).
- Ezer, T., Atkinson, L. P., Corlett, W. B. & Blanco, J. L. Gulf Stream's induced sea level rise and variability along the US mid-Atlantic coast. *J. Geophys. Res. Oceans* **118**, 685–697 (2013).
- Rosby, T., Flagg, C., Donohue, K., Sanchez-Franks, A. & Lillibridge, J. On the long-term stability of Gulf Stream transport based on 20 years of direct measurements. *Geophys. Res. Lett.* **41**, 114–120 (2014).
- Kent, E. C., Fangohr, S. & Berry, D. I. A comparative assessment of monthly mean wind speed products over the global ocean. *Int. J. Climatol.* **33**, 2520–2541 (2013).
- Farneti, R., Delworth, T. L., Rosati, A. J., Griffies, S. M. & Zeng, F. The role of mesoscale eddies in the rectification of the Southern Ocean response to climate change. *J. Phys. Oceanogr.* **40**, 1539–1557 (2010).
- Ma, X. *et al.* Western boundary currents regulated by interaction between ocean eddies and the atmosphere. *Nature* **535**, 533–537 (2016).

Acknowledgements L.M.B. and S.E. acknowledge support from the US National Science Foundation, grant OCE-0850891. The altimeter products distributed by Aviso were produced by Ssalto/Duacs, with support from Cnes (<http://www.aviso.altimetry.fr/duacs/>).

Author Contributions L.M.B. designed, obtained funding for, and led the Agulhas Current Time-series experiment and wrote and edited this paper. S.E. performed the analyses and wrote the Methods section.

Author Information Reprints and permissions information is available at www.nature.com/reprints. The authors declare no competing financial interests. Readers are welcome to comment on the online version of the paper. Correspondence and requests for materials should be addressed to L.M.B. (lbeal@rsmas.miami.edu).

METHODS

Mooring array and transports. Our *in situ* data are from the ACT mooring array, deployed across the Agulhas Current and along a satellite altimeter ground track near 34° S between April 2010 and February 2013 (Fig. 1). The array is 300 km long and oriented 15° clockwise from normal to the mean flow. Seven full-depth current-meter moorings and four current- and pressure-sensor-equipped inverted echo sounders (CPIES) were able to capture the full Agulhas jet at all times, including during meander events¹⁶. CPIES pairs provide a cost-effective estimate of full-depth geostrophic flow at the offshore end of the array. Cross-track velocity profiles are horizontally interpolated to a resolution of 1 km and integrated vertically to obtain transport per unit distance, T_x . We then define the western boundary jet transport T_{jet} as the southwestward component of T_x integrated to the first maximum of T_x beyond the half-width of the mean jet (110 km)¹⁶. We define boundary layer transport T_{box} as T_x integrated out to 219 km, the three-year mean width of the jet (Fig. 1).

Absolute dynamic topography. We use the 1-Hz unfiltered along-track absolute dynamic topography (ADT) product from Aviso. ADT is the sum of a mean dynamic topography and a sea level anomaly. The latest Aviso product uses a 20-year reference period from 1993 to 2012 to define the mean dynamic topography. Using sea level anomaly instead of ADT does not change our statistical analyses and regressions, since the two quantities differ only by a constant. In the main text we refer to ADT as sea surface height or sea level, although strictly the definition of ADT differs from sea surface height by a constant geoid. The ACT line is along altimeter track number 96 successively occupied by satellites TOPEX/Poseidon (1992–2002), Jason-1 (2002–2008), and currently Jason-2 (since 2008). During the ACT experiment, there were 105 satellite passes across the Agulhas Current, providing data between 14.6 km and 306 km offshore with a horizontal resolution of about 6.2 km. Data are available up to 8.45 km from the coast, but we discount them because they are missing 30% of the time. We estimate ADT and its slope every 1 km along the track using a local order-one polynomial regression estimator with a 24-km half-bandwidth and an Epanechnikov kernel³². Estimating slope in this way introduces less noise than differentiation and the Epanechnikov kernel minimizes the asymptotic mean square error of the resulting estimates³². A half-bandwidth of 24 km corresponds to a total window length that approaches the horizontal along-track decorrelation length scale of the flow at the ACT array (56 km)¹⁶. Varying this bandwidth by 50% does not significantly modify our results.

Transport proxies. To test the assumption of a linear and fixed relationship between *in situ* transport and sea surface height and slope for the Agulhas Current we compare the combined eigenmodes of variance of ADT and ADT slope over the full 22-year record to those of T_x over our 3 years of measurements. In each case we find four eigenmodes, of similar spatial structure, that each explain 10% or more of the variance (Extended Data Fig. 1). The dominant mode of variance at the sea surface is a broad-scale decrease or increase in sea surface slope, which is associated with a weakening or strengthening of the *in situ* transport. This is demonstrated by a strong correlation between the Principal Component time series of the first ADT mode and that of the second mode of T_x (correlation 0.76). A narrowing or broadening of the jet is reflected in the second mode of ADT and the first mode of T_x (correlation 0.84). The remaining third and fourth modes of variance in each case reflect meandering of the jet (correlations 0.72 and 0.71, respectively), while all four eigenmodes project onto mesoscale meander events. In all cases we find P values smaller than 10^{-3} and hence all correlations are highly significant. Because the Principal Component time series of T_x are serially correlated and not normally distributed, we used a nonparametric resampling method³³ to calculate one-tailed P values for the magnitude of correlation. Given the similarities between eigenmodes and the significance of correlations, we conclude that a linear relationship between sea surface variance and full-depth Agulhas transport is a fair assumption at 34° S, where the undercurrent is weak¹⁶. Hence, the variance of the current appears equivalent barotropic, in agreement with previous analyses^{17,18}.

For our preferred proxy we build nine regression models, one at each current-meter mooring and CPIES pair along the ACT array, which linearly relate the local T_x to the slope of ADT. Estimating ADT slope requires careful determination of the horizontal length scale of the flow at each site. We achieve this by using again an order-one local polynomial regression estimator with an Epanechnikov kernel³² to estimate both ADT and its slope, but this time varying the spatial bandwidth of the estimator in order to maximize the correlation between our measured T_x and the slope estimate at each mooring. This gives length scales ranging from 27 km at mooring B to 102 km at mooring G, consistent with our physical expectation of increasing length scale with increasing distance offshore. The polynomial regression estimator allows us to calculate the error variance of ADT and slope estimates at each mooring, based on the measurement errors in along-track ADT reported by Aviso. Reassuringly, we find that these error variances are at least an order of magnitude smaller than the variance of the resulting ADT and slope time series. Next, we remove outlying slope estimates by

discarding the upper and lower 0.25% of the data distribution. To fill gaps we use multivariate regression between ADT slope at the location with missing data and at surrounding locations. This technique recovers 90% of the variance of the missing data, except at mooring A, where only 68% of the variance can be explained using adjacent records. Finally, we build linear regression models between ADT slope and T_x at each of the nine mooring sites. The R^2 statistics of these models vary from 0.51 at mooring A to 0.81 at CPIES pair P4 and P5. The strongly sloping sea bed and Agulhas undercurrent (Fig. 1) probably contribute to the poorer skill of the regressions at the inshore moorings.

From the results of the regressions, we obtain T_x at each of the nine mooring locations for each satellite pass over 22 years. Subsequently, to calculate total transports from these discrete points, we fit a shape-preserving piecewise cubic Hermite interpolating polynomial function to obtain T_x at 1-km intervals across the current. We then integrate to obtain T_{jet} and T_{box} for each altimeter pass, as defined above (Fig. 2). Using instead a piecewise linear interpolation of T_x between moorings and applying a low-pass filter with a cutoff of 56 km (the decorrelation length scale given by the ACT measurements) to produce a smooth function gives alternate estimates with root-mean-square differences of 4.6 Sv for T_{jet} and 1.3 Sv for T_{box} .

A more common methodology is to build a proxy by regressing total transport onto a broad-scale sea surface slope^{14,19}. Regression based directly on along-track ADT at the ACT array is problematic, because the sea surface is strongly covarying along the length of the array, leading to large uncertainties in the regression coefficients (even though the resulting R^2 statistics of such a proxy can be high). Hence, we build a regression model using the uncorrelated Principal Components of the combined EOFs of ADT and ADT slope from above (Extended Data Fig. 1). To include as many altimeter passes as possible for the regression model, we recompute these combined EOFs for data points farther than 42.6 km from the shore to avoid missing data. The resulting EOFs differ very little from the ones presented in Extended Data Fig. 1. The regression model for both the jet and boundary transport proxies T is then:

$$T = \alpha_0 + \sum_{k \in \Omega} \alpha_k A_k(t) \quad (1)$$

where α_k are the regression coefficients estimated using the ordinary least-squares method and Ω is an ensemble of the Principal Component time series $A_k(t)$. For the ensemble we consider each eigenmode, in order of decreasing amount of variance explained, and incorporate successively only those Principal Components that increase the adjusted- R^2 statistics of our model (Equation (1)). The adjusted- R^2 statistics quantifies the amount of variance explained by a multivariate model but, in contrast to the classic R^2 statistics, attempts to correct for the explained variance that occurs by chance from adding a random variate to the model. For T_{box} this procedure selects Principal Components 1 and 2 (correlated with transport at 0.85 and 0.22 respectively, with P values $< 10^{-3}$ and 0.09), and for T_{jet} Principal Components 1, 2 and 3 (correlated at 0.49, 0.27 and 0.20, respectively, with P values $< 10^{-3}$, 0.015 and 0.05).

The resulting proxy for T_{box} explains 76% of the variance, while in the case of T_{jet} the proxy explains only 39% of the variance (Extended Data Fig. 2). The poor performance of the jet proxy is probably because it is defined from only the southwestward flow, while sea level variance along the whole array reflects the net flow. Estimating the linear trends of the two time series we find that the boundary layer transport appears to be strengthening at a significant rate ($\pm 95\%$ confidence interval) of -4.9 ± 2.0 Sv per decade, while the jet transport has a weaker and insignificant trend of -1.4 ± 1.5 Sv per decade (Extended Data Fig. 2). The boundary layer proxy trend fulfils prior expectations, based on warming sea surface temperatures and strengthening winds over the region^{9,10}. However, this strengthening is inconsistent with trends in sea surface height across the current (Fig. 3). The structures and nodes of the eigenmodes of sea level and slope (Extended Data Fig. 1) are fixed in space and seem to be unable to capture the change in structure of the boundary layer over time. Throughout the 22-year record, the trend patterns explain never more than 8% of the local variance and the EOFs are virtually unchanged when recomputed after detrending the data. Simply put, a proxy based on a single regression with total transport does not allow for a broadening of the current.

Spectral estimates and annual cycle. Power spectral densities of the proxies T_{jet} and T_{box} are estimated using the adaptive multitaper method with five Slepian tapers³⁴. This method exhibits less variance than other common methods and is routinely employed for climate time series analysis³⁵. Using three or seven tapers, of the Slepian form or other forms, does not qualitatively change our results. Significant spectral peaks at the 95% confidence level were identified using a test for periodicities within a red background spectrum³⁶. Since T_{jet} has less energy than T_{box} at periods longer than 100 days (Fig. 2), we expect decadal signals and trends to be more clearly detected in the jet transport. Annual cycles are obtained by calculating daily means using the Nadaraya–Watson kernel estimator with a

Gaussian kernel of half-width 30 days³². 95% confidence intervals are based on the assumption of a normal distribution of the estimates.

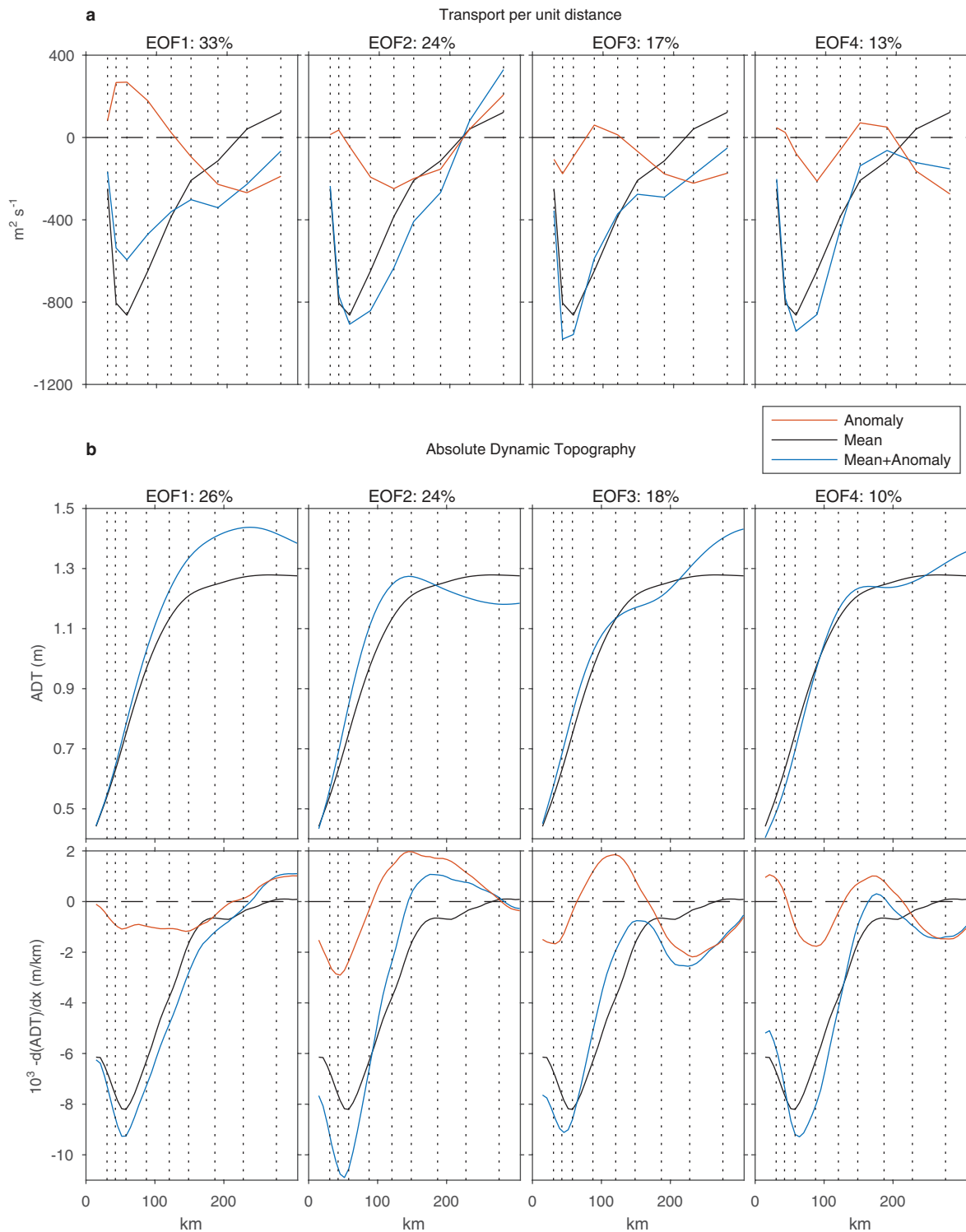
Trends in sea level and kinetic energy. Trends in sea level (Fig. 3) are calculated using along-track satellite altimeter data from Aviso and from the new Sea Level Climate Change Initiative (CCI) product³⁷, which is optimized for long-term signals. For kinetic energy across the Agulhas Current (Fig. 4) we use the post-2014 geostrophic velocity maps from Aviso, which are derived from a two-satellite, merged, delayed-time product. For long-term signals it is important to use the two-satellite product because it ingests a consistent amount of data over time, avoiding the introduction of sampling bias that may cause spurious trends in variance. TKE is defined as half the sum of the squared horizontal components of velocity. MKE is calculated from the total velocity time series by low-pass filtering using a sliding quadratic window with half-bandwidth of 18 months. EKE is calculated from the velocity residuals obtained by subtracting the low-pass-filtered velocities from the total velocities. These calculations result in an interannually evolving MKE, and an EKE which captures variability at timescales of less than 18 months. Although mapped satellite altimeter products have difficulties resolving boundary flows that are narrow and close to the coast, reassuringly we find that at the ACT array peak MKE occurs close to the mean *in situ* Agulhas Current core (Fig. 4a).

Code availability. MATLAB scripts used for our analyses and figures are available upon request from S.E.

Data availability. The *in situ* mooring data from the ACT experiment (velocities from current meters and acoustic Doppler current profilers; sound speed, pressure

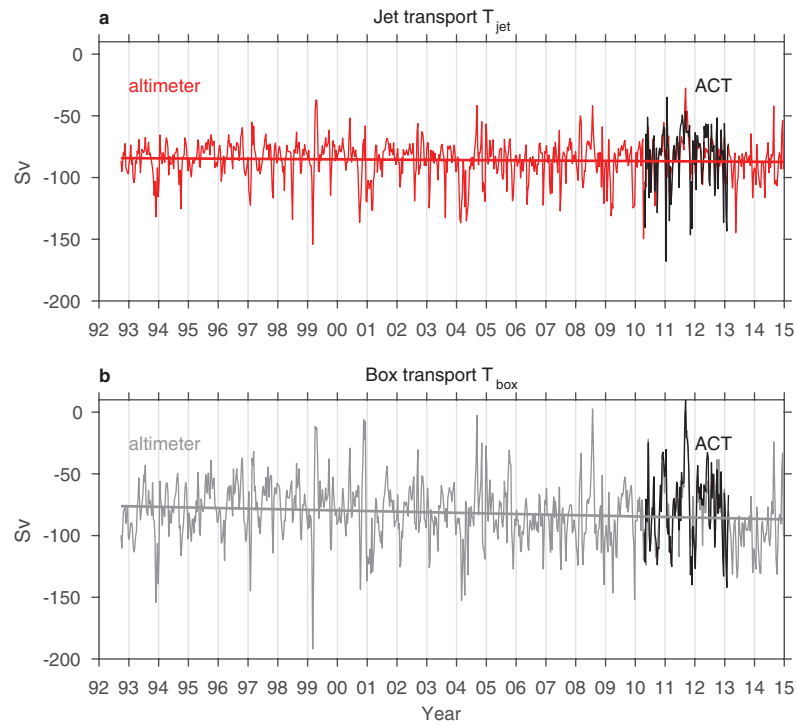
and bottom velocity from CPIES) are archived with the NOAA National Centers for Environmental Information (<https://www.ncei.noaa.gov>), with accession numbers 0156669 and 0156605. Aviso along-track Absolute Dynamic Topography data are accessible through <http://www.aviso.altimetry.fr/en/data/products/sea-surface-height-products/global/adt-h.html#c5139>. Maps of absolute dynamic topography and absolute geostrophic velocities are accessible through <http://www.aviso.altimetry.fr/en/data/products/sea-surface-height-products/global/madt-h-uv.html>. The CCI altimeter along-track data correspond to the Fundamental Climate Data Record product (http://dx.doi.org/10.5270/esa-sea_level_cci-1993_2014-v_1.1-201512) generated by the Sea Level Climate Change Initiative project (<http://www.esa-sealevel-cci.org/>).

32. Fan, J. & Gijbels, I. *Local Polynomial Modelling and its Applications: Monographs on Statistics and Applied Probability* Vol. 66 (CRC Press, 1996).
33. Ebisuzaki, W. A method to estimate the statistical significance of a correlation when the data are serially correlated. *J. Clim.* **10**, 2147–2153 (1997).
34. Thomson, D. Spectrum estimation and harmonic analysis. *Proc. IEEE* **70**, 1055–1096 (1982).
35. Grimm, E. C. *et al.* A 50,000-year record of climate oscillations from Florida and its temporal correlation with the Heinrich events. *Science* **261**, 198 (1993).
36. Percival, D. B. & Walden, A. T. *Spectral Analysis for Physical Applications* (Cambridge Univ. Press, 1993).
37. Ablain, M. *et al.* Improved sea level record over the satellite altimetry era (1993–2010) from the climate change initiative project. *Ocean Sci.* **11**, 67–82 (2015).



Extended Data Figure 1 | Spatiotemporal variance of oceanic transport and sea surface slope are similar across the Agulhas Current. a, First four eigenmodes of the transport per unit distance from the ACT array. **b,** First four combined eigenmodes of sea surface height and slope, from

Aviso along-track absolute dynamic topography (ADT) from satellite altimetry. Note that the ADT gradient is positive across most of the array, but is shown as negative for comparison with the southward Agulhas Current transports in **a**. Black dotted lines depict mooring positions.



Extended Data Figure 2 | Agulhas Current transport proxies based on regressions of total transport with sea surface eigenmodes. a, Proxy for jet or stream-wise transport T_{jet} . **b,** Proxy for boundary layer transport T_{box} . The three years of *in situ* transports from the ACT array are shown as black lines. The trends of these two proxies are inconsistent, owing to observed broadening of the jet.